

Charm-quark mass effects in NRQCD matching coefficients and the leptonic decay of the $\Upsilon(1S)$ meson

Manuel Egner¹, Matteo Fael¹, Jan Piclum², Kay Schönwald¹ and Matthias Steinhauser¹

¹*Institut für Theoretische Teilchenphysik, Karlsruhe Institute of Technology (KIT),
76128 Karlsruhe, Germany*

²*Center for Particle Physics Siegen, Theoretische Physik 1, Universität Siegen, 57068 Siegen, Germany*

 (Received 24 May 2021; accepted 30 August 2021; published 27 September 2021)

We compute two-loop corrections to the vector current matching coefficient involving two heavy quark masses. The result is applied to the computation of the $\Upsilon(1S)$ decay width into an electron or muon pair. We complement the next-to-next-to-next-to-leading order corrections of M. Beneke, *et al.* [*Phys. Rev. Lett.* **112**, 151801 (2014)] by charm quark mass effects up to second order in perturbation theory. Furthermore, we apply the formalism to $\Gamma(J/\Psi \rightarrow \ell^+\ell^-)$ and compare to the experimental data.

DOI: 10.1103/PhysRevD.104.054033

I. INTRODUCTION

Bottomonia, the bound states of a bottom and an antibottom quark, are excellent systems to investigate the dynamics of bound states in QCD. On the experimental side, there exist precise measurements of their properties. And on the theoretical side, the large mass of the bottom quark means that perturbation theory can be applied. This is in particular the case for the $\Upsilon(1S)$ meson. Nevertheless, its description is complicated by the fact that aside from the bottom-quark mass m_b (the hard scale), there are two more relevant scales: the typical momentum and energy of the quarks, which are of order $m_b v$ (the soft scale) and $m_b v^2$ (the ultrasoft scale), respectively. The $\Upsilon(1S)$ is a non-relativistic bound state, where the relative velocity v of the quark and antiquark is small, which means that these scales are well separated. It is then convenient to use an effective theory for the description of this multiscale problem. Starting from QCD, we first integrate out the hard modes to arrive at nonrelativistic QCD (NRQCD). In a second step, we integrate out the soft modes and potential gluons with ultrasoft energies and soft momenta to arrive at potential NRQCD (PNRQCD). At each step, one has to determine the Wilson or matching coefficients of the corresponding effective theory, which are the couplings of the effective operators. For comprehensive reviews on this topic, we refer to [1,2].

The main focus of this paper is the matching coefficient c_v of the vector current in NRQCD. Among other

observables, it contributes to the decay rate of an $\Upsilon(1S)$ to a lepton-antilepton pair. In PNRQCD and to next-to-next-to-next-to-leading order (N^3LO) accuracy, the decay rate is given by the formula [3],

$$\Gamma(\Upsilon(1S) \rightarrow \ell^+\ell^-) = \frac{4\pi\alpha^2}{9m_b^2} |\psi_1(0)|^2 c_v \times \left[c_v - \frac{E_1}{m_b} \left(c_v + \frac{d_v}{3} \right) + \dots \right], \quad (1)$$

where α is the fine structure constant and m_b the bottom-quark pole mass. E_1 and $\psi_1(0)$ are the binding energy and the wave function at the origin of the $(b\bar{b})$ system. For convenience, we provide the leading order results, which are given by

$$|\psi_1^{LO}(0)|^2 = \frac{8m_b^3\alpha_s^3}{27\pi}, \quad E_1^{LO} = -\frac{4m_b\alpha_s^2}{9}. \quad (2)$$

The matching coefficient c_v of the leading current is known at the three-loop level [4–6] for the case of one massive quark and n_f massless quarks. d_v is the matching coefficient of the subleading $b\bar{b}$ current in NRQCD. Since it is multiplied by E_1 , it is only required at the one-loop level. This result can be found in Ref. [2]. Together with the N^3LO results for the energy levels and the wave function at the origin [2,3,7], this made it possible to evaluate the decay rate at N^3LO in Ref. [8].

One approximation that was made in Ref. [8] was to treat the charm quark as massless. The aim of this paper is to go beyond this approximation and include the corrections due to the charm-quark mass at next-to-next-to-leading order (NNLO). If we consider the charm-quark mass m_c to be formally of the order of the hard scale m_b , the charm quark

Published by the American Physical Society under the terms of the Creative Commons Attribution 4.0 International license. Further distribution of this work must maintain attribution to the author(s) and the published article's title, journal citation, and DOI. Funded by SCOAP³.

has to be integrated out of QCD, leading to NRQCD with two heavy quarks with different masses. All NRQCD matching coefficients will then receive contributions due to m_c . However, at NNLO, only c_v is affected. Thus, we have to compute the fermionic contribution to the two-loop corrections to c_v for a second nonzero quark mass. The analytic result for this contribution completes the two-loop evaluation of c_v and together with its application to $\Gamma(\Upsilon(1S) \rightarrow \ell^+ \ell^-)$ constitutes the main result of our paper.

Another possibility to include the charm-quark mass effects is to consider m_c to be soft. In this case, the charm quark is integrated out of NRQCD. Then there is no contribution to c_v but instead to the matching coefficients of PNRQCD, which are the potentials in the Schrödinger equation describing the $(b\bar{b})$ system. At NNLO, only the Coulomb potential is affected (see Sec. 3.5 of Ref. [9]). Thus, the m_c dependence then enters in the wave function and binding energy. We will compare the results of these two approaches.

The remainder of the paper is organized as follows: In the next section, we describe the calculation of c_v , and in Sec. III, the discussion is extended to external axial-vector, scalar, and pseudoscalar currents, where in addition to the nonsinglet also the singlet contributions have to be considered. In Sec. IV, we provide updated predictions for $\Gamma(\Upsilon(1S) \rightarrow \ell^+ \ell^-)$, and in Sec. V, we consider the decay of the J/Ψ and provide predictions of $\Gamma(J/\Psi \rightarrow \ell^+ \ell^-)$ up to N³LO. Our conclusions are presented in Sec. VI. In the Appendix, analytic results for all matching coefficients up to two loops, which are not presented in the main part of the paper, are provided. The Supplemental Material to this paper [10] contains computer-readable expressions of all matching coefficients and all master integrals, which we compute in this paper.

II. TWO-LOOP MATCHING COEFFICIENT FOR THE VECTOR CURRENT WITH TWO MASSES

The matching coefficient for the vector current is defined via

$$j_v^i = c_v \tilde{j}_v^i + \mathcal{O}\left(\frac{1}{m_q}\right), \quad (3)$$

where m_q is the heavy quark mass and j_v^i and \tilde{j}_v^i are currents defined in the full (QCD) and effective (NRQCD) theory. They are given by

$$j_v^\mu = \bar{\psi} \gamma^\mu \psi, \quad \tilde{j}_v^i = \phi \sigma^i \chi, \quad (4)$$

where ϕ and χ are two-component spinors. Note that in the heavy quark limit the zeroth component of j_v^μ is of order $1/m_q^2$.

A convenient approach to compute c_v is based on the so-called threshold expansion [11,12], which is applied to the vertex corrections of a vector current and a heavy quark-antiquark pair, Γ_v . Denoting by Z_2 , the on shell quark wave function renormalization constant, one obtains the equation [5],

$$Z_2 \Gamma_v(q_1, q_2) = c_v \frac{\tilde{Z}_2}{Z_v} \tilde{\Gamma}_v + \mathcal{O}\left(\frac{1}{m_q}\right). \quad (5)$$

Note that the vector current in QCD has a vanishing anomalous dimension whereas \tilde{Z}_v deviates from 1 at order α_s^2 . It gets contributions from the color factors C_F^2 and $C_A C_F$, which are not considered in this paper. The momenta q_1 and q_2 in Eq. (5) correspond to the outgoing momenta of the quark and antiquark, which are considered on shell. Furthermore, we have $(q_1 + q_2)^2 = 4m_q^2$, a consequence of the threshold expansion.

The quantity Γ_v is conveniently obtained with the help of projectors applied to the vertex function Γ^μ . It is straightforward to show that one gets

$$\Gamma_v = \text{Tr}[P_\mu^v \Gamma^{v,\mu}], \quad (6)$$

with

$$P_\mu^v = \frac{1}{8(d-1)m_q^2} \left(-\frac{\not{q}}{2} + m_q\right) \gamma_\mu \left(\frac{\not{q}}{2} + m_q\right), \quad (7)$$

where $q = q_1 + q_2$.

In Fig. 1, we show sample diagrams contributing to c_v up to two-loop order. The main focus of this work is the Feynman diagram in Fig. 1(a) where the quark in the closed loop has mass m_2 . For the computation of this diagram we proceed as follows.

- (i) We apply the projector in Eq. (7) to the amplitude of the Feynman diagram in Fig. 1 and take the traces. After decomposing the numerator in terms of denominator factors we obtain scalar integrals of the form,¹

$$I(n_1, \dots, n_6) = \int \frac{d^d k}{(2\pi)^d} \frac{d^d l}{(2\pi)^d} \frac{(q \cdot l)^{-n_6}}{(-k^2)^{n_1} (m_q^2 - (\frac{q}{2} + k)^2)^{n_2} (m_q^2 - (-\frac{q}{2} + k)^2)^{n_3} (m_2^2 - (k+l)^2)^{n_4} (m_2^2 - l^2)^{n_5}}. \quad (8)$$

¹In the denominators, we omit $i\epsilon$, which could easily be reconstructed by shifting the squared momenta according to $p^2 \rightarrow p^2 + i\epsilon$.

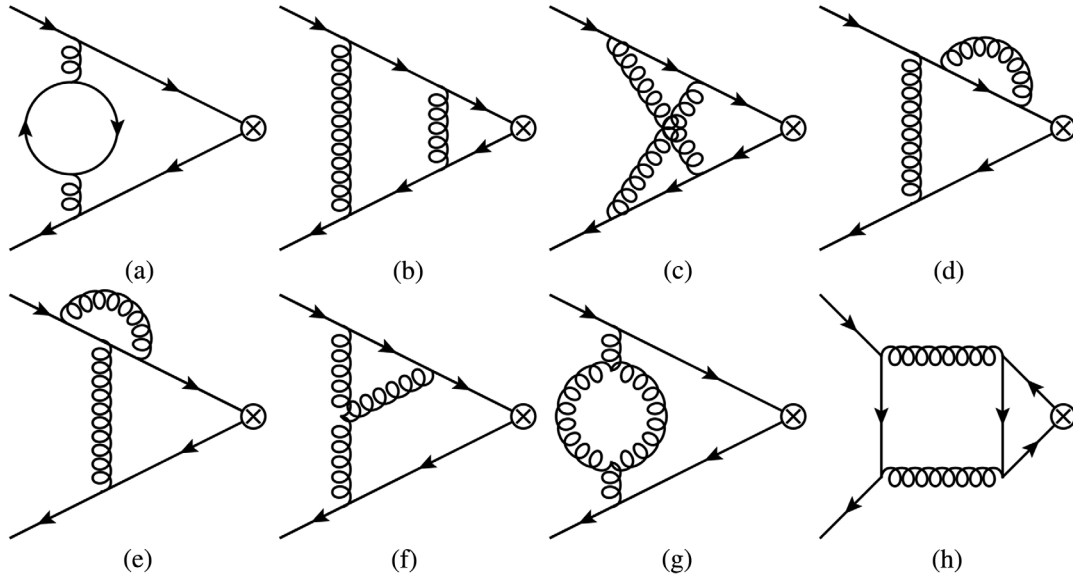


FIG. 1. Sample Feynman diagrams (a)–(h) contributions to the matching coefficient c_v . Straight and curly lines represent quarks and gluons, respectively. The cross represents the external current. The main focus of this paper is diagram (a) where the quark in the closed loop has mass m_2 . Note that the singlet diagram shown in (h) vanishes for an external vector current. However, for an axial-vector, scalar, or pseudoscalar current it is nonzero.

- (ii) In a next step, we perform a partial fraction decomposition in order to arrive at integral families where the propagator factors are linearly independent. In our case, this is achieved with the help of

$$\int \frac{d^d k}{(m_q^2 - (\frac{q}{2} + k)^2)(m_q^2 - (-\frac{q}{2} + k)^2)} = \int \frac{d^d k}{(-k^2)(m_q^2 - (-\frac{q}{2} + k)^2)}, \quad (9)$$

which is valid for $q^2 = 4m_q^2$.

- (iii) We pass the resulting integrals to FIRE [13] and LiteRed [14] and perform a reduction to four master integrals, which are given by

$$\begin{aligned} I_1 &= \int \frac{d^d k}{(2\pi)^d} \frac{d^d l}{(2\pi)^d} \frac{1}{(m_2^2 - k^2)(m_2^2 - l^2)}, \\ I_2 &= \int \frac{d^d k}{(2\pi)^d} \frac{d^d l}{(2\pi)^d} \frac{1}{(m_q^2 - k^2)(m_2^2 - l^2)}, \\ I_3 &= \int \frac{d^d k}{(2\pi)^d} \frac{d^d l}{(2\pi)^d} \frac{1}{(m_q^2 - (-\frac{q}{2} + k)^2)(m_2^2 - (k+l)^2)(m_2^2 - l^2)}, \\ I_4 &= \int \frac{d^d k}{(2\pi)^d} \frac{d^d l}{(2\pi)^d} \frac{1}{(m_q^2 - (-\frac{q}{2} + k)^2)^2(m_2^2 - (k+l)^2)(m_2^2 - l^2)}. \end{aligned} \quad (10)$$

Their graphical representation can be found in Fig. 2.

- (iv) Next, we introduce the variable $x = m_2/m_q$ and establish differential equations for the master integrals of the form,

$$\frac{d\vec{I}}{dx} = M \cdot \vec{I}, \quad (11)$$

where the matrix M decomposes into two 1×1 and one 2×2 blocks. The differential equations are brought to ϵ form using CANONICA [15],

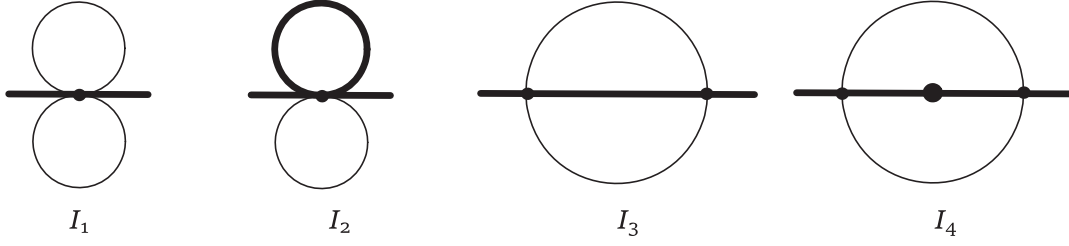


FIG. 2. Graphical representation of the master integrals of Eq. (10). Thick and thin solid lines represent scalar propagators with mass m_q and m_2 , respectively. The external momentum is always $q/2$ with $(q/2)^2 = m_q^2$.

$$\frac{d\vec{J}}{dx} = \epsilon \vec{M} \cdot \vec{J}, \quad (12)$$

where the matrix \vec{M} does not depend on ϵ and $\vec{I} = T \cdot \vec{J}$. This allows us to compute \vec{J} order-by-order in ϵ and express the result in terms of iterated integrals, which in our case, can be expressed in terms of harmonic polylogarithms [16].

- (v) In order to fix the boundary conditions, we consider the limits $x \rightarrow 0$ and $x \rightarrow 1$. This is necessary since in each individual limit some of the integration constants drop out. Alternatively, it would be possible to solve the differential equation to higher order in ϵ . The values of \vec{I} for $x = 0$ and $x = 1$ are used to determine the integration constants in \vec{J} .

We want to remark that we use a general QCD gauge parameter ξ for our computation. The independence of our final result from ξ is a welcome cross-check. Our results for the master integrals agree with those given in Appendix B of Ref. [17].

For the renormalization of our two-loop contribution, we need the two-loop corrections to the on shell wave function

renormalization constant. The analytic results for the contribution involving m_2 can be found in Refs. [17–21]. Furthermore, the one-loop counterterm for α_s is needed. At this point, we use Eq. (5) in order to extract c_v .

For the fermionic contributions to c_v , it is convenient to introduce $n_f = n_h + n_m + n_l$, where $n_h = 1$ and $n_m = 1$ label the contributions with closed massive quark loops with mass m_q and m_2 , respectively. n_l counts the massless quarks. Using this notation, we can cast the result for c_v in the form,

$$c_v = 1 - 2C_F \frac{\alpha_s^{(n_l+n_m)}(\mu)}{\pi} + \left(\frac{\alpha_s^{(n_l+n_m)}(\mu)}{\pi} \right)^2 c_v^{(2)} + \mathcal{O}(\alpha_s^3), \quad (13)$$

where $\alpha_s^{(n_l+n_m)}(\mu)$ is the strong coupling constant where the heavy quark with mass m_q is decoupled from the running of α_s . The m_2 -independent contributions to $c_v^{(2)}$ can be found in Refs. [4,5,22]. The new contribution proportional to n_m reads

$$\begin{aligned} c_v^{(2)}|_{m_2} = n_m C_F T_F & \left[\frac{71}{72} + \frac{35x^2}{24} + \pi^2 \left(\frac{3}{32x} - \frac{11x}{48} - \frac{17x^3}{32} + \frac{2x^4}{9} \right) + \frac{1}{24} (23 + 19x^2) H_0 + \frac{4}{3} x^4 H_0^2 \right. \\ & + \left(\frac{3}{16x} - \frac{11x}{24} - \frac{17x^3}{16} + \frac{4x^4}{3} \right) H_0 H_1 + \left(-\frac{3}{16x} + \frac{11x}{24} + \frac{17x^3}{16} - \frac{4x^4}{3} \right) H_{0,1} \\ & \left. + \left(\frac{3}{16x} - \frac{11x}{24} - \frac{17x^3}{16} - \frac{4x^4}{3} \right) H_{-1,0} + \frac{2}{3} \log \left(\frac{\mu^2}{m_2^2} \right) \right], \end{aligned} \quad (14)$$

where $H_{i\dots} = H_{i\dots}(x)$ and $H_{i\dots}(x)$ are harmonic polylogarithms (HPLs) [16]. Note that for $x \rightarrow 1$, we reproduce the known result for $m_2 = m_q$, which is given by

$$c_v^{(2)}|_{m_2} \xrightarrow{x \rightarrow 1} n_m C_F T_F \left[\frac{22}{9} - \frac{2\pi^2}{9} + \frac{2}{3} \log \left(\frac{\mu^2}{m_q^2} \right) + \left(-\frac{10}{3} + \frac{37\pi^2}{72} \right) y + \left(2 - \frac{\pi^2}{12} \right) y^2 + \mathcal{O}(y^3) \right], \quad (15)$$

with $y = x - 1$. However, in the limit $x \rightarrow 0$, we do not obtain the massless fermion contribution but recover the well-known Coulomb singularity, which is regulated by the mass m_2 . For small m_2 , we have

$$c_v^{(2)}|_{m_2} \xrightarrow{x \rightarrow 0} n_m C_F T_F \left[\frac{3\pi^2}{32x} + \frac{11}{18} + \frac{2}{3} \log \left(\frac{\mu^2}{m_q^2} \right) - \frac{11\pi^2}{48} x + \frac{7}{3} x^2 - \frac{17\pi^2}{32} x^3 + \mathcal{O}(x^4) \right]. \quad (16)$$

In the application we discuss in Sec. IV, we need c_v expressed in term of $\alpha_s^{(n_l=3)}$, which means that we have to decouple the charm quark from the running of α_s . As a consequence, μ^2 is effectively replaced by m_2^2 in Eqs. (14), (15), and (16).

$$c_v^{(2)} = -44.72 + 0.17n_h + 0.41n_l + 1.75n_m + \log\left(\frac{\mu^2}{m_q^2}\right)[-20.13 + 0.44(n_l + n_m)], \quad (17)$$

where the contributions originating from the closed massless, bottom, and charm quark loops are marked by $n_l = 3$, $n_h = 1$, and $n_m = 1$, respectively. One observes that the coefficient of n_m is more than a factor 4 times larger than the coefficients of n_l and n_h . Thus, the contribution of the heavy quark with mass m_2 is larger than the contributions of the heavy quark with mass m_q and all three massless quarks combined.

III. TWO-LOOP TWO-MASS MATCHING COEFFICIENTS FOR AXIAL-VECTOR, SCALAR, AND PSEUDOSCALAR CURRENTS

In this section, we consider further external currents, which are of phenomenological relevance, and compute the corresponding matching coefficients between QCD and NRQCD to two-loop order. Such currents have, in contrast to the vector case, both nonsinglet and singlet contributions. The latter are characterized by the fact that the external current does not directly couple to the quarks in the final state but only through the exchange of two gluons. A sample Feynman diagram is shown in Fig. 1(h).

We write the two-loop corrections in the form,

$$c_k^{(2)} = c_{k,\text{nonsing}}^{(2)} + c_{k,\text{sing}}^{(2)}, \quad (18)$$

where $k \in \{a, s, p\}$ stands for an axial vector, scalar, or pseudoscalar. All two-loop corrections, which involve only one mass scale, have been computed in Ref. [22]. In this paper, we concentrate on the diagrams where a second massive quark in a closed loop is present which concerns both the nonsinglet and the singlet contribution.

In analogy to Eq. (3), we define the additional currents in QCD via

$$\begin{aligned} j_a^\mu &= \bar{\psi}\gamma^\mu\gamma_5\psi, \\ j_s &= \bar{\psi}\psi, \\ j_p &= \bar{\psi}i\gamma_5\psi. \end{aligned} \quad (19)$$

The anomalous dimension of j_a^μ is zero. For the scalar and pseudoscalar current we have for the corresponding renormalization constant $Z_s = Z_p = Z_m$, where Z_m is the (on shell) mass renormalization constant.

Let us finally investigate the numerical effect of the new contribution. We specify to the bottom-charm system and use $m_2 = m_c = 1.65$ GeV and $m_q = m_b = 5.1$ GeV for the pole masses of the charm and bottom quarks. This leads to

In NRQCD, the currents read [22]

$$\begin{aligned} \tilde{j}_a^k &= \frac{1}{2m}\phi^\dagger[\sigma^k, \vec{p} \cdot \vec{\sigma}]\chi, \\ \tilde{j}_s &= -\frac{1}{m}\phi^\dagger\vec{p} \cdot \vec{\sigma}\chi, \\ \tilde{j}_p &= -i\phi^\dagger\chi, \end{aligned} \quad (20)$$

where $k = 1, 2, 3$. Furthermore, we have $j_a^0 = i\tilde{j}_p$, which constitutes an alternative way to compute the matching coefficient c_p . Note the presence of the momentum \vec{p} , which is the relative momentum of the external quark and antiquark, in the definition of the axial-vector and scalar current. Thus, an expansion in p has to be performed in order to obtain the loop corrections to the corresponding matching coefficients.

The matching equation in (5) also holds for the other currents after the obvious replacements of Γ_v , \tilde{Z}_v , and $\tilde{\Gamma}_v$ and the introduction of $Z_{s,p}$ for the scalar and pseudoscalar currents.

For the pseudoscalar current and the zero component of the axial vector, the momentum p is zero, and the calculation proceeds in close analogy to the vector case. In fact, we have [22].

$$\begin{aligned} \Gamma_p &= \text{Tr}[P^{(p)}\Gamma^{(p)}], \\ \Gamma_{a,0} &= \text{Tr}[P_\mu^{(a,0)}\Gamma^{(a),\mu}], \end{aligned} \quad (21)$$

with

$$\begin{aligned} P^{(p)} &= \frac{1}{8m_q^2}\left(-\frac{\not{p}}{2} + m_q\right)\gamma_5\left(\frac{\not{p}}{2} + m_q\right), \\ P_\mu^{(a,0)} &= -\frac{1}{8m_q^2}\left(-\frac{\not{p}}{2} + m_q\right)\gamma_\mu\gamma_5\left(\frac{\not{p}}{2} + m_q\right). \end{aligned} \quad (22)$$

For the axial-vector and scalar cases, there are similar equations to Eq. (21). The expansion in p (up to linear order) is conveniently realized by choosing $q_1 = q/2 + p$ and $q_2 = q/2 - p$, which implies $q \cdot p = 0$. Thus, the projectors are more complicated and are given by

$$\begin{aligned}
 P_{(a,i),\mu} &= -\frac{1}{8m_q^2} \left\{ \frac{1}{d-1} \left(-\frac{\not{q}}{2} + m_q \right) \gamma_\mu \gamma_5 \left(-\frac{\not{q}}{2} + m_q \right) \right. \\
 &\quad \left. - \frac{1}{d-2} \left(-\frac{\not{q}}{2} + m_q \right) \frac{m_q}{p^2} ((d-3)p_\mu + \gamma_\mu \not{p}) \gamma_5 \left(\frac{\not{q}}{2} + m_q \right) \right\}, \\
 P_{(s)} &= \frac{1}{8m_q^2} \left\{ \left(-\frac{\not{q}}{2} + m_q \right) \mathbf{1} \left(-\frac{\not{q}}{2} + m_q \right) + \left(-\frac{\not{q}}{2} + m_q \right) \frac{m_q}{p^2} \not{p} \left(\frac{\not{q}}{2} + m_q \right) \right\}. \tag{23}
 \end{aligned}$$

After the application of the projectors and the expansion in p , we can set $p = 0$ and $q^2 = 4m_q^2$.

The calculation of the nonsinglet contribution is in close analogy to the vector case; see Sec. II. In particular, it is possible to use anticommuting γ_5 . Furthermore, we can map the scalar integrals contributing to Γ_x after the application of the projector to the same integral families, and we thus end up with the same master integrals.

The singlet contribution is more involved and a few comments are in order. Let us first mention that a nonzero contribution for the scalar and pseudoscalar currents is only obtained for massive quarks in the closed fermion loop. Furthermore, for the axial-vector current, an effective current formed by the difference of the upper and lower component of a given quark doublet should be considered in order to guarantee the cancellation of anomaly-like contributions. For example, for the top-bottom doublet, we have

$$j_a^\mu = \bar{t} \gamma^\mu \gamma_5 t - \bar{b} \gamma^\mu \gamma_5 b. \tag{24}$$

In practice, this means that we have a quark with mass m_q in the final state, and we consider both a massless quark and a quark with mass m_2 in the closed quark loop and take the difference.

In the singlet diagrams, we treat γ_5 according to the prescription of Ref. [23]. In the Feynman diagrams, we apply for the axial-vector and pseudoscalar couplings the replacements,

$$\begin{aligned}
 \gamma^\mu \gamma_5 &\rightarrow \frac{i}{3!} \epsilon^{\mu\nu\rho\sigma} \gamma_\nu \gamma_\rho \gamma_\sigma, \\
 \gamma_5 &\rightarrow \frac{i}{4!} \epsilon^{\mu\nu\rho\sigma} \gamma_\mu \gamma_\nu \gamma_\rho \gamma_\sigma. \tag{25}
 \end{aligned}$$

We perform the same substitution also in the corresponding projectors. Afterwards, we strip off the two ϵ tensors and interpret the product in d dimensions. This allows us to perform the calculation in close analogy to the scalar current.

The remaining calculation of the singlet diagrams proceeds as outlined in the previous section. After applying a partial fraction decomposition, we can map all integrals in our amplitude to two integral families, which are given by

$$J_1(\vec{n}) = \int \frac{d^d k}{(2\pi)^d} \frac{d^d l}{(2\pi)^d} \frac{1}{(m_2^2 - (k + \frac{q}{2})^2)^{n_1} (m_2^2 - (k - \frac{q}{2})^2)^{n_2} (m_2^2 - (k - l)^2)^{n_3} (m_q^2 - l^2)^{n_4} (-l + \frac{q}{2})^2)^{n_5}}, \tag{26}$$

$$J_2(\vec{n}) = \int \frac{d^d k}{(2\pi)^d} \frac{d^d l}{(2\pi)^d} \frac{1}{(m_2^2 - (k + \frac{q}{2})^2)^{n_1} (m_2^2 - (k - \frac{q}{2})^2)^{n_2} (m_2^2 - (k - l)^2)^{n_3} (-l + \frac{q}{2})^2)^{n_4} (-l - \frac{q}{2})^2)^{n_5}}. \tag{27}$$

The reduction to master integrals using FIRE [13] and LiteRed [14] leads to 12 master integrals, which are shown in Fig. 3. In a next step, we establish differential equations in the variable t defined by $x = 2t/(1+t^2)$. In this new variable, the differential equation can be brought into ϵ form with the help of CANONICA [15]. We expand the solution including terms of order ϵ since some of the master integrals have $1/\epsilon$ poles in the prefactor. The differential equations are integrated with the help of HarmonicSums [24] in terms of cyclotomic harmonic polylogarithms over the alphabet,

$$f_0(\tau) = \frac{1}{\tau}, \quad f_1(\tau) = \frac{1}{1-\tau}, \quad f_{-1}(\tau) = \frac{1}{1+\tau}, \quad f_{\{4,1\}}(\tau) = \frac{\tau}{1+\tau^2}. \tag{28}$$

Alternatively, one could factorize the denominators over the complex numbers and arrive at Goncharov polylogarithms. The boundary conditions are obtained from the single-scale master integrals needed for the two-loop calculation of Refs. [22,25]. For the master integrals with dots, the naive $m_2 = 0$ limit is not enough, and we have to consider the asymptotic expansion around $m_2 = 0$, which can be obtained easily from one-dimensional Mellin-Barnes representations or a diagrammatic large momentum expansion of the corresponding Feynman integrals. In a second approach, we use the algorithm described in

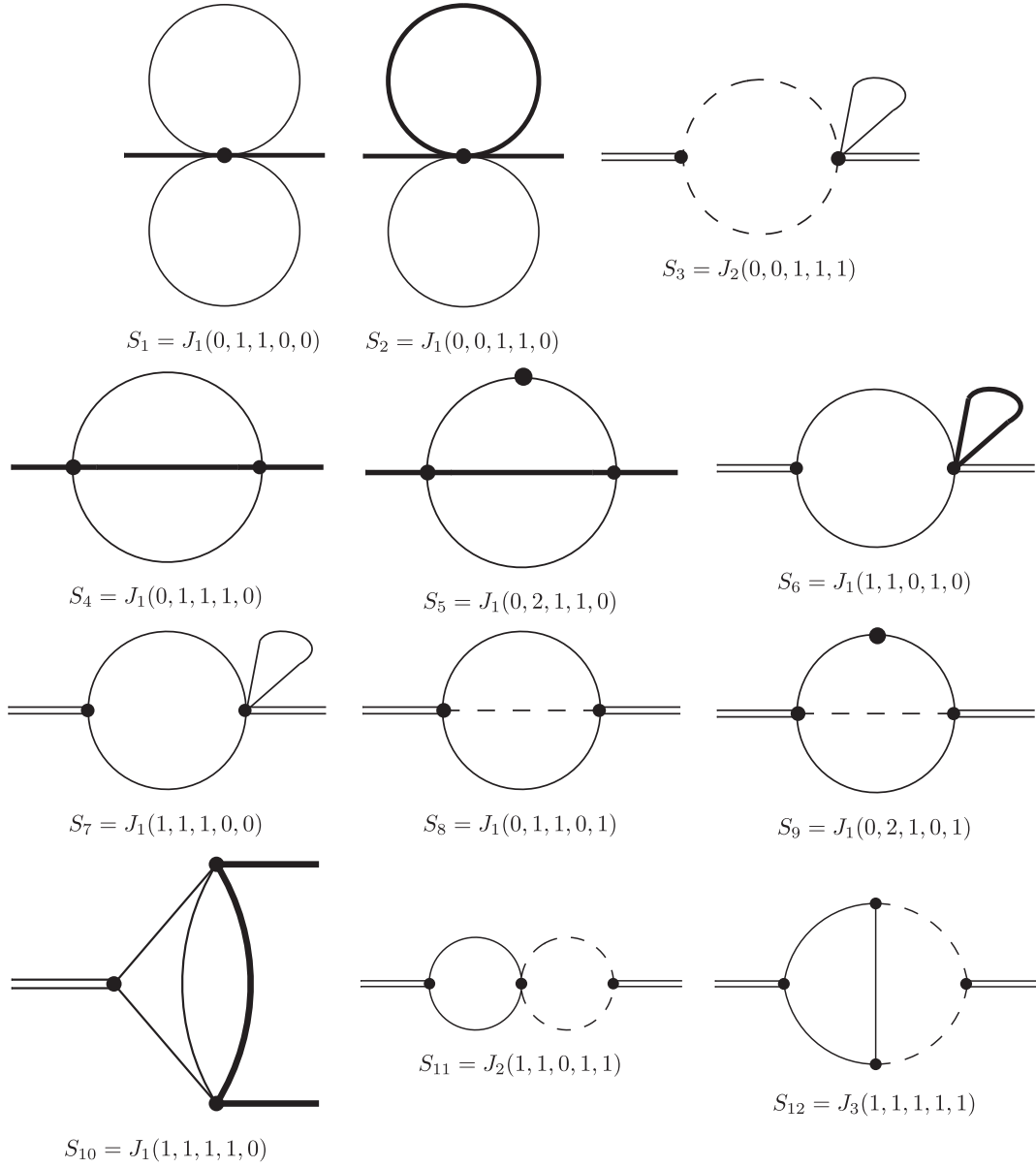


FIG. 3. Master integrals needed for the calculation of the singlet diagrams. Thick and thin lines represent scalar propagators with mass m_q and m_2 , respectively. Dashed lines represent massless scalar propagators. External double lines represent the momentum q and thick lines the momentum $q/2$ with $q^2 = 4m_q^2$.

[26] to solve the differential equations in the variable x without going into an ϵ form first. For the implementation, we additionally make use of Sigma [27] and OreSys [28]. This approach introduces the square-root valued letter $\sqrt{1 - \tau^2/\tau}$. Both results agree after the above mentioned variable transformation. We compute the ϵ expansion of all

master integrals up to the order, which is needed to obtain the $\mathcal{O}(\epsilon)$ terms of the matching coefficients.

After inserting the master integrals into the integration-by-parts-reduced amplitude, we obtain for the two-loop singlet contribution to the matching coefficient of the scalar current the following expression:

$$\begin{aligned}
 c_{s,\text{sing}}^{(2)}|_{m_2} = n_m C_F T_F & \left[\frac{4t}{3(1+t^2)} + \pi^2 \left[\frac{t(1-28t^2-35t^4)}{18(1+t^2)^3} + \frac{4t^3 H_1}{3(1+t^2)^3} + \frac{2t(3+2t^2+3t^4)H_{\{4,1\}}}{3(1+t^2)^3} + \frac{4t^3 H_{-1}}{(1+t^2)^3} \right] \right. \\
 & + \log(2) \left[-\frac{8t^3 H_0}{3(1+t^2)^2} + \left(-\frac{4t}{3(1+t^2)} + \frac{32t^3 H_{-1}}{3(1+t^2)^3} \right) H_1 + \frac{16t^3 H_1^2}{3(1+t^2)^3} + \frac{4t H_{-1}}{3(1+t^2)} + \frac{16t^3 H_{-1}^2}{3(1+t^2)^3} \right] \\
 & + \frac{4t^3 H_0}{(1+t^2)^2} + \frac{4t^3(3+4t^2)H_0^2}{3(1+t^2)^3} + \left(\frac{4t(3t^2-5)H_0}{3(1+t^2)^2} + \frac{16t^3 H_0^2}{3(1+t^2)^3} \right) H_1 + \frac{16t^3 H_0 H_1^2}{3(1+t^2)^3} \\
 & + \left(-\frac{4t}{1+t^2} + \frac{8t(1-t^2)H_0}{3(1+t^2)^2} - \frac{8t(3+2t^2+3t^4)H_0^2}{3(1+t^2)^3} \right) H_{\{4,1\}} + \left(\frac{4t(5-3t^2)}{3(1+t^2)^2} - \frac{32t^3 H_0}{(1+t^2)^3} \right. \\
 & - \left. \frac{32t^3 H_1}{3(1+t^2)^3} \right) H_{0,1} + \left(\frac{8t(3t^2-1)}{3(1+t^2)^2} + \frac{8t(3+2t^2+3t^4)H_0}{(1+t^2)^3} \right) H_{0,\{4,1\}} + \frac{8t H_{1,\{4,1\}}}{3(1+t^2)} \\
 & + \left(\frac{4t(5-3t^2)}{3(1+t^2)^2} + \frac{64t^3 H_0}{3(1+t^2)^3} + \frac{32t^3 H_1}{3(1+t^2)^3} \right) H_{-1,0} - \left(\frac{8t}{3(1+t^2)} + \frac{64t^3 H_1}{3(1+t^2)^3} \right) H_{-1,\{4,1\}} \\
 & + \frac{160t^3 H_{0,0,1}}{3(1+t^2)^3} - \frac{8t(3-2t+3t^2)(3+2t+3t^2)H_{0,0,\{4,1\}}}{3(1+t^2)^3} + \frac{32t^3 H_{0,1,1}}{3(1+t^2)^3} - \frac{64t^3 H_{1,1,\{4,1\}}}{3(1+t^2)^3} \\
 & - \frac{160t^3 H_{-1,0,0}}{3(1+t^2)^3} - \frac{32t^3 H_{-1,0,1}}{3(1+t^2)^3} + \frac{64t^3 H_{-1,\{4,1\},1}}{3(1+t^2)^3} + \frac{32t^3 H_{-1,-1,0}}{3(1+t^2)^3} - \frac{64t^3 H_{-1,-1,\{4,1\}}}{3(1+t^2)^3} \\
 & - \frac{2t \log^2(2)}{3(1+t^2)} - \frac{t(3+4t^2+3t^4)\zeta(3)}{(1+t^2)^3} + i\pi \left\{ \frac{2\pi^2 t^3}{3(1+t^2)^3} + \frac{2t^3}{(1+t^2)^2} + \left(\frac{4t^3(4+5t^2)}{3(1+t^2)^3} + \frac{32t^3 H_{-1}}{3(1+t^2)^3} \right) H_0 \right. \\
 & - \left. \left(\frac{8t(1-t^2)}{3(1+t^2)^2} - \frac{16t^3 H_0}{3(1+t^2)^3} \right) H_1 + \left(\frac{4t(1-t^2)}{3(1+t^2)^2} - \frac{8t(3+2t^2+3t^4)H_0}{3(1+t^2)^3} \right) H_{\{4,1\}} \right. \\
 & \left. + \frac{8t(1-t^2)H_{-1}}{3(1+t^2)^2} - \frac{16t^3 H_{0,1}}{(1+t^2)^3} + \frac{4t(3+2t^2+3t^4)H_{0,\{4,1\}}}{(1+t^2)^3} - \frac{16t^3 H_{-1,0}}{(1+t^2)^3} + \frac{2t(1-t^2)\log(2)}{3(1+t^2)^2} \right\} \Bigg], \quad (29)
 \end{aligned}$$

with $t = (1 - \sqrt{1-x^2})/x$ and $H_{\bar{a}} = H_{\bar{a}}(t)$. The imaginary part of the matching coefficient is displayed in the last three lines of Eq. (29). For the expansion around $x = 0$, we find

$$\begin{aligned}
 c_{s,\text{sing}}^{(2)}|_{m_2,x \rightarrow 0} = n_m C_F T_F & \left[x \left(\frac{2}{3} + \frac{\pi^2}{36} - \frac{\log^2(2)}{3} - \frac{3\zeta(3)}{2} \right) + x^3 \left(-\frac{7}{24} - \frac{\pi^2}{12} + \frac{7}{12} \log(x) - \frac{3 \log(2)}{4} - \frac{1}{3} \log(2) \log(x) \right. \right. \\
 & \left. \left. + \frac{\log^2(2)}{3} + \frac{\zeta(3)}{4} \right) + i\pi \left\{ \frac{1}{3} x \log(2) + x^3 \left(\frac{3}{8} + \frac{\pi^2}{12} + \frac{1}{6} \log(x) - \frac{\log(2)}{3} \right) \right\} + \mathcal{O}(x^4) \right]. \quad (30)
 \end{aligned}$$

As expected, this contribution to the matching coefficient is zero for vanishing quark mass in the closed triangle. Note that mass corrections are linear in m_2 . On the other hand, for $x \rightarrow 1$ $c_{s,\text{sing}}^{(2)}|_{m_2}$ approaches a constant. Higher order expansion terms are conveniently expressed in terms of $y = 1 - x$ and are given by

$$\begin{aligned}
 c_{s,\text{sing}}^{(2)}|_{m_2,x \rightarrow 1} = n_m C_F T_F & \left[\frac{2}{3} - \frac{29\pi^2}{72} - \log(2) + \frac{2}{3} \pi^2 \log(2) + y \left(-\frac{2}{3} + \frac{53\pi^2}{72} + \log(2) - \pi^2 \log(2) - \frac{21\zeta(3)}{4} \right) \right. \\
 & - \frac{1}{9} \pi^2 \sqrt{2} y^{3/2} + y^2 \left(-\frac{5}{2} + \frac{5\pi^2}{48} + 4 \log(2) + \frac{1}{2} \pi^2 \log(2) + \frac{63\zeta(3)}{8} \right) - \frac{7}{30} \pi^2 \frac{y^{5/2}}{\sqrt{2}} \\
 & + i\pi \left\{ \frac{1}{2} - y \left(\frac{1}{2} - \frac{\pi^2}{4} \right) - y^{3/2} \sqrt{2} \left(\frac{23}{9} - \frac{8}{9} \log(y) - \frac{14}{9} \log(2) \right) - y^2 \left(2 + \frac{3}{8} \pi^2 \right) \right. \\
 & \left. + y^{5/2} \sqrt{2} \left(\frac{1591}{300} - \frac{6}{5} \log(y) - \frac{79}{30} \log(2) \right) \right\} + \mathcal{O}(y^3) \Bigg]. \quad (31)
 \end{aligned}$$

The expressions for the pseudo-scalar and axial-vector currents can be found in the Appendix, where we also show the nonsinglet terms.

IV. $\Gamma(\Upsilon(1S) \rightarrow \ell^+ \ell^-)$ AND FINITE CHARM QUARK MASS

In Ref. [8], the charm quark has been treated as massless, and the decay rate has been expressed in terms of $\alpha_s^{(n_l)}(\mu)$ with $n_l = 4$. In the following, we discuss the additional ingredients needed for the finite charm quark mass terms up to and including NNLO. As mentioned in the Introduction, we consider two scenarios:

- (A) m_c is hard and the charm quark is integrated out when matching QCD to NRQCD. In this approach, we express $\Gamma(\Upsilon(1S) \rightarrow \ell^+ \ell^-)$ in terms of $\alpha_s^{(3)}(\mu)$. There are finite- m_c effects in the matching coefficient c_v starting from two loops. These corrections have been computed in Sec. II. There are no finite- m_c corrections to the binding energy and the wave function at the origin.
- (B) m_c is soft, and thus, the charm quark is a dynamical scale within NRQCD. We express $\Gamma(\Upsilon(1S) \rightarrow \ell^+ \ell^-)$ in terms of $\alpha_s^{(4)}(\mu)$. In this approach, charm mass effects to bound-state energies and wave functions are needed. They are known at NLO [29] and NNLO [9,30]. We use the expressions given in Ref. [9].

In case the decay rate shall be expressed in terms of the potential subtracted mass, the charm quark mass effects are needed to NNLO [9].

All necessary expressions for this scenario are available in the program `QQbar_threshold` [31]. In both scenarios, charm mass effects to the relation between the $\overline{\text{MS}}$ (which we use as input), and on shell bottom quark mass are taken into account. They are known to three-loop order [19,21].

In scenario A, we assume that m_c is parametrically of the order of m_b . In such a situation, both m_b and m_c have to be decoupled from the running of α_s and $\alpha_s^{(3)}$ is used as an expansion parameter. In fact, it has been observed (see, e.g., Ref. [32]) that, e.g., the finite- m_c terms to the $\overline{\text{MS}}$ -on shell relation of the bottom quark are quite sizeable and do not converge in case $\alpha_s^{(4)}$ is used as parameter. On the other

hand, charm quark mass corrections are small and well convergent for $\alpha_s^{(3)}$.

To arrive at the new result for $\Gamma(\Upsilon(1S) \rightarrow \ell^+ \ell^-)$, we proceed as follows. Our starting point is the expression derived in Ref. [8], where $\alpha_s^{(4)}$ has been used as expansion parameter. For the number of massless quarks, we have $n_l = 4$. We restore the dependence on (massless) charm quarks and write $n_l = n'_l + n_m$ with $n'_l = 3$ and $n_m = 1$. In scenario B, we can simply add the finite- m_c terms from the binding energy and wave function. This modifies the coefficient of n_m such that in the limit $m_c \rightarrow 0$ the coefficient of n'_l is recovered.

In scenario A, we interpret the result of Ref. [8] in the $n_l = 3$ -flavor PNRQCD with an expansion parameter $\alpha_s^{(3)}$. Finite- m_c effects enter in Eq. (1) only via the matching coefficient c_v (cf. Sec. II), which also has to be expressed in terms of $\alpha_s^{(3)}$.

As mentioned in the Introduction, the description of the decay rate $\Gamma(\Upsilon(1S) \rightarrow \ell^+ \ell^-)$ within PNRQCD is a multi-scale problem, and thus, it would in principle be desirable to provide a corresponding separation of the factorization and renormalization scales. Whereas at lower orders this has been achieved (see, e.g., Refs. [33,34]), it is not yet known at N³LO. Thus, in our analysis, we identify the various scales by μ and discuss the variation of this common scale, which provides an estimate of the numerical effect.

We are now in the position to provide numerical results for the decay rate. For the numerical evaluation, we use $\alpha(2m_b) = 1/132.3$ [35], $\alpha_s^{(5)}(M_Z) = 0.1179(10)$ [36] and the renormalization scale $\mu = 3.5$ GeV. We use the program `RunDec` [37] to evolve the coupling with five-loop accuracy and obtain $\alpha_s^{(4)}(3.5 \text{ GeV}) = 0.2388$ and $\alpha_s^{(3)}(3.5 \text{ GeV}) = 0.2297$, respectively. Furthermore, we compute the pole mass $m_b = 5.059$ GeV in the four-loop approximation from the $\overline{\text{MS}}$ value $\bar{m}_b(\bar{m}_b) = 4.163(16)$ GeV given in Ref. [38]. In our expressions, we renormalize the charm quark in the $\overline{\text{MS}}$ scheme at the renormalization scale $\mu_c = 3$ GeV and use $\bar{m}_c(3 \text{ GeV}) = 0.993$ GeV [38]. Our results in the two scenarios read

$$\begin{aligned}
 \Gamma(\Upsilon(1S) \rightarrow \ell^+ \ell^-)|_{\text{pole,A}} &= \frac{2^5 \alpha^2 \alpha_s^3 m_b}{3^5} [1 + 0.374 + (0.916 + 0.020_{c_v}) - 0.032] \\
 &= 1.041 + 0.009_{c_v} \\
 &= [1.051 \pm 0.047(\alpha_s)_{-0.217}^{+0.007}(\mu)] \text{ keV}, \\
 \Gamma(\Upsilon(1S) \rightarrow \ell^+ \ell^-)|_{\text{pole,B}} &= \frac{2^5 \alpha^2 \alpha_s^3 m_b}{3^5} [1 + (0.259 + 0.037_{m_c}) + (0.869 + 0.039_{m_c}) - 0.178] \\
 &= 1.011 + 0.039_{m_c} \\
 &= [1.050 \pm 0.045(\alpha_s)_{-0.155}^{+0.024}(\mu)] \text{ keV},
 \end{aligned} \tag{32}$$

where the four terms in the first lines of the two equations refer to the LO, NLO, NNLO, and N³LO results. At NNLO and in scenario B also at NLO, we display the contributions from a finite charm quark mass separately. We remark that the finite- m_c terms of $c_v^{(2)}$ (see subscript c_v), which are computed in Sec. II, amount to about 2% of the NNLO coefficient, and they are of the same order of magnitude as the N³LO contribution. In scenario B, the m_c effects at NLO and NNLO (see subscript m_c) are of the same order of magnitude and amount to about 15% and 5% of the corresponding m_c -independent coefficient. The scale uncertainty in the last line of Eq. (32) is computed from the variation of μ in the range $\mu \in [3, 10]$ GeV. We also show the uncertainty induced by $\delta\alpha_s^{(5)}(M_Z) = 0.001$. The variation of all other parameters leads to significantly smaller uncertainties.

It is interesting to note that both scenario A and scenario B lead to the same final prediction at N³LO although the contributions from the various orders is different. We observe a notable discrepancy to the experimental result, which is given by $\Gamma(\Upsilon(1S) \rightarrow e^+e^-)|_{\text{pole}} = 1.340(18)$ keV. We also want to mention a recent lattice evaluation [39], where the value $\Gamma(\Upsilon(1S) \rightarrow e^+e^-) = 1.292(37)(3)$ keV has been reported.

In Fig. 4, we show the dependence of $\Gamma(\Upsilon(1S) \rightarrow e^+e^-)|_{\text{pole,A}}$ on μ successively including higher order corrections. The solid black line corresponds to the N³LO prediction. We observe that the inclusion of higher order corrections clearly stabilizes the perturbative predictions for $\mu \gtrsim 3$ GeV. Furthermore, it is interesting to note that the third-order correction vanishes close to the value of μ , where the N³LO curve has a maximum. The dashed black curve corresponds to the N³LO prediction of scenario B. The

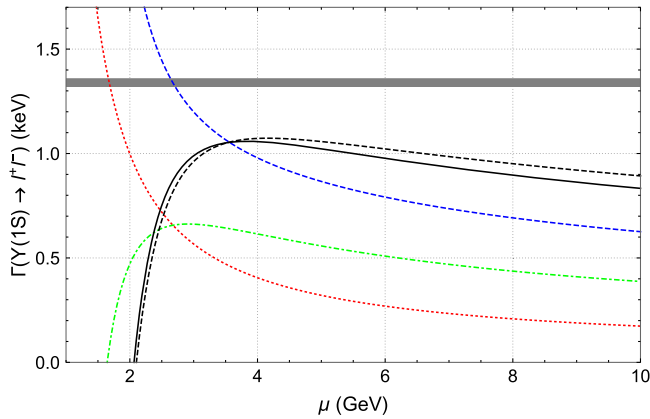


FIG. 4. The decay rate obtained from scenario A in the pole scheme as a function of the renormalization scale μ . Dotted (red), dash-dotted (green), short-dashed (blue), and solid (black) lines correspond to LO, NLO, NNLO, and N³LO predictions. At N³LO, we also show the result from scenario B as black dashed curve. The horizontal bar denotes the experimental value for $\Gamma(\Upsilon(1S) \rightarrow e^+e^-)$.

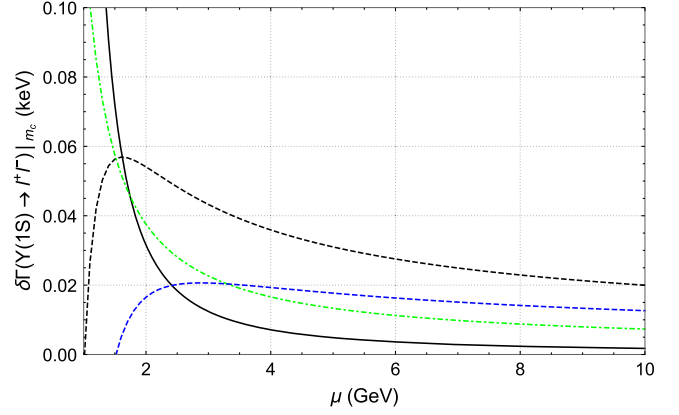


FIG. 5. Charm quark mass dependent terms for scenario A (solid black curve) and B (dashed black curve). For scenario B, the NLO and NNLO contributions are shown also separately; see green and blue curves.

overall shape is very similar to the corresponding curve of scenario A. However, it is remarkable that the two N³LO lines cross the NNLO curve for the same value of μ .

For illustration, we show in Fig. 5 the charm quark mass dependent terms of $\Gamma(\Upsilon(1S) \rightarrow \ell^+\ell^-)$ as a function of the renormalization scale. The solid black curve corresponds to the NNLO term of scenario A marked by c_v . For scenario B, we show the NLO and NNLO contributions as green dash-dotted and blue dashed curves. Their sum is the black dashed line. One observes that for $\mu = 3.5$ GeV [which is the choice of Eq. (32)] both terms of scenario B are about twice as big as the one in scenario A. In fact, over the whole range of μ , the charm dependent terms of scenario B are significantly larger than those of scenario A. Note that for $\mu \approx 1.7$ GeV, the NNLO scenario B contribution turns zero, and the whole correction is given by the NLO term. The observed behavior is in analogy to Ref. [32], where it was argued that for the $\overline{\text{MS}}$ -on shell relation the charm mass-dependent terms are small and well convergent in case $\alpha_s^{(3)}$ is used as expansion parameter.

In Fig. 6, we show $\Gamma(\Upsilon(1S) \rightarrow e^+e^-)|_{\text{pole,A}}$ as a function of $\alpha_s^{(5)}(M_Z)$. One observes that the third-order band is embedded in the NNLO band, which can be interpreted as good convergence of the perturbative corrections. Note that we do not recompute the bottom pole mass when varying α_s .

It is well-known that the pole mass suffers from so-called renormalon ambiguities. They are avoided by choosing a properly defined so-called threshold mass. Such masses have the advantages that they have nice convergence properties (as the $\overline{\text{MS}}$ mass) and that they can also be used for the description of bound-state properties. In the following, we want to consider the potential-subtracted (PS) mass scheme [40] as an example and discuss the perturbative corrections to $\Gamma(\Upsilon(1S) \rightarrow \ell^+\ell^-)$.

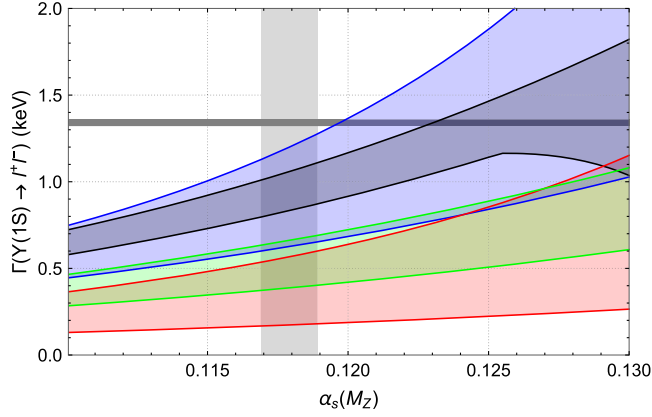


FIG. 6. The decay rate obtained from scenario A in the pole scheme as a function of $\alpha_s(M_Z)$ at LO (red, bottom), NLO (green, middle), NNLO (blue, top), and N³LO (black, inner top band). The bands denote the variation of μ between 3 GeV and 10 GeV. The horizontal bar denotes the experimental value, while the vertical bar denotes the world average of the strong coupling constant, $\alpha_s(M_Z) = 0.1179(10)$.

Explicit results for the relation between the pole mass and the PS mass to n th order can be derived from the n -loop expression for the Coulomb potential (see, for example, Ref. [41]). For scenario A, we use this relation for $n = 3$ and $n_l = 3$, since in this scenario finite charm-quark mass effects are only included in the relation between the $\overline{\text{MS}}$ mass and pole mass. In scenario B, however, we also have to include charm-mass effects in the relation between the

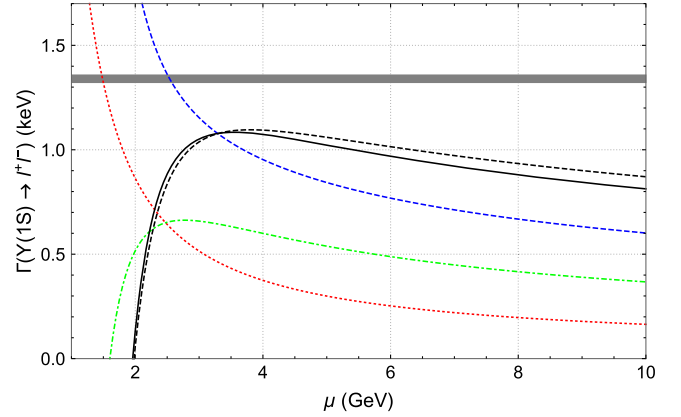


FIG. 7. The decay rate obtained from scenario A in the PS scheme as a function of the renormalization scale μ . Dotted (red), dash-dotted (green), short-dashed (blue), and solid (black) lines correspond to LO, NLO, NNLO, and N³LO predictions. At N³LO, we also show the result from scenario B as black dashed curve. The horizontal bar denotes the experimental value for $\Gamma(\Upsilon(1S) \rightarrow e^+e^-)$.

pole mass and PS mass for $n = 1$ and $n = 2$. The latter can be found in Appendix B of Ref. [9].

The numerical (input) value for the PS mass is conveniently obtained from $\bar{m}_b(\bar{m}_b) = 4.163$ GeV. Using N³LO accuracy, we obtain for the two scenarios $m_b^{\text{PS}}|_A = 4.520$ GeV and $m_b^{\text{PS}}|_B = 4.484$ GeV, respectively, where the factorization scale μ_f is set to 2 GeV. For the decay rate of the $\Upsilon(1S)$, we obtain

$$\begin{aligned}
 \Gamma(\Upsilon(1S) \rightarrow \ell^+\ell^-)|_{\text{PS,A}} &= \frac{2^5 \alpha_s^2 \alpha_s^3 m_b}{3^5} [1 + 0.485 + (1.001 + 0.017_{c_v}) + 0.125] \\
 &= 1.076 + 0.007_{c_v} \\
 &= [1.083 \pm 0.053(\alpha_s)_{-0.270}^{+0.001}(\mu)] \text{ keV}, \\
 \Gamma(\Upsilon(1S) \rightarrow \ell^+\ell^-)|_{\text{PS,B}} &= \frac{2^5 \alpha_s^2 \alpha_s^3 m_b}{3^5} [1 + (0.374 + 0.042_{m_c}) + (0.939 + 0.048_{m_c}) - 0.029] \\
 &= 1.050 + 0.041_{m_c} \\
 &= [1.091 \pm 0.052(\alpha_s)_{-0.218}^{+0.006}(\mu)] \text{ keV}.
 \end{aligned} \tag{33}$$

The final predictions for the decay rate are close to those in the on shell scheme [cf. Eqs. (32)] and agree well within the uncertainties. However, the transition from the pole to the PS mass leads to a significant redistribution among the various perturbative orders. For example, in scenario A the N³LO term in the PS scheme is about 4 times larger as compared to the on shell scheme but has a different sign. Similarly, in scenario B, the N³LO coefficient gets reduced by a factor of 6.

For completeness, we show in Figs. 7 and 8, the dependence of $\Gamma(\Upsilon(1S) \rightarrow \ell^+\ell^-)$ in the PS scheme on

μ and $\alpha_s^{(5)}(M_Z)$, respectively. The behavior of the various perturbative orders and the interpretation of the results is very similar to Figs. 4 and 6.

As mentioned above, in our analysis, we have identified the factorization and renormalization scales. As can be seen from Figs. 4 and 7, the variation of μ leads to relatively big effects which suggests a separation of the scales. However, such an analysis is beyond the scope of this paper.

The inclusion of the finite- m_c effects leads to the same conclusions as in Ref. [8]: The perturbative predictions for $\Gamma(\Upsilon(1S) \rightarrow \ell^+\ell^-)$ are well under control, but there is a

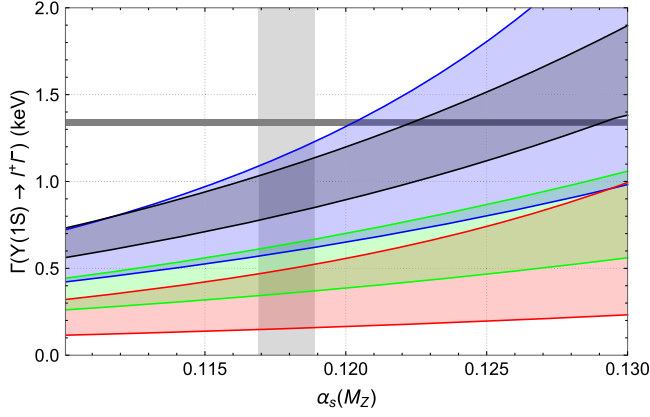


FIG. 8. The decay rate obtained from scenario A in the PS scheme as a function of $\alpha_s(M_Z)$ at LO (red, bottom), NLO (green, middle), NNLO (blue, top), and N³LO (black, inner top band). The bands denote the variation of μ between 3 GeV and 10 GeV. The horizontal bar denotes the experimental value, while the vertical bar denotes the world average of the strong coupling constant, $\alpha_s(M_Z) = 0.1179(10)$.

discrepancy with respect to the experimental result. In [8], one can find an extensive discussion on possible non-perturbative effects. However, no clear conclusion can be drawn, and it remains an open question whether a full quantitative understanding of the decay rate based on perturbative and nonperturbative QCD is possible.

It is interesting to apply our formulae to the excited ($b\bar{b}$) states with $n = 2$ and $n = 3$. For higher n , the average momentum of the bound system is reduced. However, for illustration purposes, we still use $\mu = 3.5$ GeV. Furthermore, we restrict ourselves to the pole scheme and approach A. We obtain $\Gamma(Y(2S) \rightarrow \ell^+\ell^-)|_{\text{pole,A}} = 0.161$ keV and $\Gamma(Y(3S) \rightarrow \ell^+\ell^-)|_{\text{pole,A}} = 0.0565$ keV, which has to be compared to the experimental results $\Gamma(Y(2S) \rightarrow \ell^+\ell^-)|_{\text{exp}} = 0.612$ keV and $\Gamma(Y(3S) \rightarrow \ell^+\ell^-)|_{\text{exp}} = 0.443$ keV. One observes a large deviation,

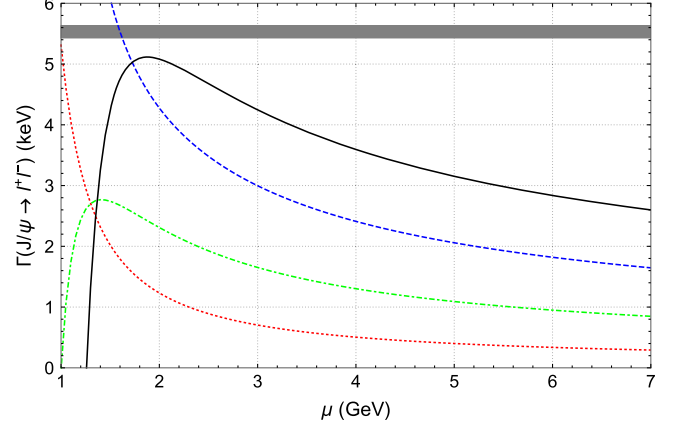


FIG. 9. The decay rate $\Gamma(J/\Psi \rightarrow \ell^+\ell^-)$ in the OS scheme as a function of the renormalization scale μ . Dotted (red), dash-dotted (green), short-dashed (blue), and solid (black) lines correspond to LO, NLO, NNLO, and N³LO prediction. The horizontal bar denotes the experimental value for $\Gamma(J/\Psi \rightarrow e^+e^-)$.

which is probably due to even larger nonperturbative contributions.

V. $\Gamma(J/\Psi \rightarrow \ell^+\ell^-)$ AT N³LO

In this section, we apply scenario A to the decay of the J/Ψ meson to massless leptons. In general, the application to charm bound states is questionable, since the ultrasoft scale in PNRQCD is smaller than Λ_{QCD} . Furthermore, even the hard scale (m_c) is below 2 GeV. Nevertheless, it is interesting to study the perturbative behavior and to compare with the experimental result.

We work with an on shell charm quark mass value $m_c = 1.65$ GeV and choose $\mu = 2$ GeV for the renormalization scale. This leads to $\alpha_s^{(3)}(2 \text{ GeV}) = 0.2943$. For the decay rate, we have

$$\begin{aligned} \Gamma(J/\Psi \rightarrow \ell^+\ell^-)|_{\text{pole}} &= \frac{42^5 \alpha^2 \alpha_s^3 m_c}{3^5} [1 + 0.875 + (1.596 - 0.001_{c_v}) + 0.654] \\ &= [5.08 \pm 0.35(\alpha_s)_{-2.25}^{+0.03}(\mu)] \text{ keV}, \end{aligned} \quad (34)$$

where the scale uncertainty is computed from the variation of μ in the range $\mu \in [1.5, 6]$ GeV. The NNLO term with the subscript c_v originates from the two-loop contribution to the charm quark vector current with a closed bottom quark. Although the perturbative series does not converge, it is instructive to compare to the experimental result. This is done in Fig. 9, where $\Gamma(J/\Psi \rightarrow \ell^+\ell^-)$ is shown as a function of μ . It is interesting to notice that there is agreement between the N³LO prediction and the

experimental result $\Gamma(J/\Psi \rightarrow \ell^+\ell^-)|_{\text{exp}} = 5.53 \pm 0.10$ keV [36] close to the value of μ , where the N³LO curve has a maximum, and thus, the derivative with respect to μ vanishes. Furthermore, for this value of μ , the third-order corrections are quite small, as can be seen from Eq. (34). Note that the N³LO corrections vanish for $\mu = 1.724$ GeV. For this value of the renormalization scale, we have $\Gamma(J/\Psi \rightarrow \ell^+\ell^-)|_{\text{pole}} = 5.03$ keV. From Fig. 9, we also observe that even the N³LO curve shows a sizable

dependence on μ . Furthermore, one notices that below $\mu \approx 1.5 \text{ GeV} \approx m_c$ perturbation theory breaks down. For completeness, let us mention that for $n = 2$ we have $\Gamma(\Psi(2S) \rightarrow \ell^+ \ell^-) = 0.865 \text{ keV}$, which has to be compared to the experimental result $\Gamma(\Psi(2S) \rightarrow \ell^+ \ell^-)|_{\text{exp}} = 2.34 \text{ keV}$.

We want to remark that a similar feature has been observed in Ref. [42], where next-to-leading logarithmic (NLL) corrections to the hyperfine splitting of heavy quark-antiquark bound states have been considered. The application to the 1S charmonium state shows good agreement for values of the renormalization scale, where the NLL prediction has a maximum. The perturbative uncertainties are sizeable, as for the J/Ψ decay rate.

A recent lattice computation of the leptonic decay width is given by $\Gamma(J/\Psi \rightarrow e^+ e^-) = 5.637 \pm 0.049$ [43], in agreement with the experimental value [36].

VI. CONCLUSIONS

In this paper, we consider the matching coefficients between QCD and NRQCD of external vector, axial-vector, scalar, and pseudoscalar currents. We compute all two-loop contributions that involve two mass scales, one from the external quarks and one present in a closed fermion loop. Whereas for the vector current only nonsinglet contributions have to be considered, there are also singlet contributions for the other three currents. We present analytic results including terms of order ϵ , which are of relevance for a future three-loop calculation.

In Secs. IV and V, we apply our results for the vector current to the leptonic decay rates of the lowest spin-1 heavy-quark-anti-quark mesons, $\Upsilon(1S)$ and J/Ψ , and provide update numerical predictions. We discuss the decay rate $\Gamma(\Upsilon(1S) \rightarrow \ell^+ \ell^-)$, including charm quark mass effects, both in the three- and four-flavor scheme and for the heavy quark masses defined both in the on shell and PS scheme. Although at the central scale, the third-order corrections are small and the scale dependence is significantly reduced when going from NNLO to N³LO, we observe a discrepancy with respect to the experimental result, which to date is not understood. As a final remark, we want to mention that a closer look to the charm quark mass dependent terms suggests that their convergence properties improve after decoupling of m_c from the running of α_s and using $\alpha_s^{(3)}$ as an expansion parameter.

ACKNOWLEDGMENTS

This research was supported by the Deutsche Forschungsgemeinschaft (DFG, German Research Foundation) under Grant No. 396021762—TRR 257 “Particle Physics Phenomenology after the Higgs Discovery.”

APPENDIX: ANALYTIC RESULTS FOR $c_a, c_s,$ AND c_p

In this Appendix, we present analytic results for the two-mass matching coefficients for axial-vector, scalar, and pseudoscalar external currents. The nonsinglet results are given by

$$\begin{aligned}
c_{a,\text{nonsing}}^{(2)}|_{m_2} &= n_m C_F T_F \left[\frac{37}{72} + \frac{41x^2}{24} + \pi^2 \left(\frac{1}{32x} - \frac{5x}{48} - \frac{19x^3}{32} + \frac{2x^4}{9} \right) + \frac{1}{24} (13 + 25x^2) H_0 + \frac{4}{3} x^4 H_0^2 \right. \\
&\quad + \left(\frac{1}{16x} - \frac{5x}{24} - \frac{19x^3}{16} + \frac{4x^4}{3} \right) H_0 H_1 + \left(-\frac{1}{16x} + \frac{5x}{24} + \frac{19x^3}{16} - \frac{4x^4}{3} \right) H_{0,1} \\
&\quad \left. + \left(\frac{1}{16x} - \frac{5x}{24} - \frac{19x^3}{16} - \frac{4x^4}{3} \right) H_{-1,0} + \frac{1}{3} \log \left(\frac{\mu^2}{m_2^2} \right) \right], \\
c_{s,\text{nonsing}}^{(2)}|_{m_2} &= n_m C_F T_F \left[-\frac{1}{72} + \frac{27x^2}{8} + \pi^2 \left(\frac{1}{32x} + \frac{x}{16} - \frac{35x^3}{32} + \frac{x^4}{3} \right) + \frac{1}{24} (5 + 57x^2) H_0 + 2x^4 H_0^2 \right. \\
&\quad + \left(\frac{1}{16x} + \frac{x}{8} - \frac{35x^3}{16} + 2x^4 \right) H_0 H_1 + \left(-\frac{1}{16x} - \frac{x}{8} + \frac{35x^3}{16} - 2x^4 \right) H_{0,1} \\
&\quad \left. + \left(\frac{1}{16x} + \frac{x}{8} - \frac{35x^3}{16} - 2x^4 \right) H_{-1,0} + \frac{1}{6} \log \left(\frac{\mu^2}{m_2^2} \right) \right], \\
c_{p,\text{nonsing}}^{(2)}|_{m_2} &= n_m C_F T_F \left[\frac{11}{24} + \frac{25x^2}{8} + \pi^2 \left(\frac{3}{32x} - \frac{x}{16} - \frac{33x^3}{32} + \frac{x^4}{3} \right) + \frac{1}{8} (5 + 17x^2) H_0 + 2x^4 H_0^2 \right. \\
&\quad + \left(\frac{3}{16x} - \frac{x}{8} - \frac{33x^3}{16} + 2x^4 \right) H_0 H_1 + \left(-\frac{3}{16x} + \frac{x}{8} + \frac{33x^3}{16} - 2x^4 \right) H_{0,1} \\
&\quad \left. + \left(\frac{3}{16x} - \frac{x}{8} - \frac{33x^3}{16} - 2x^4 \right) H_{-1,0} + \frac{1}{2} \log \left(\frac{\mu^2}{m_2^2} \right) \right], \tag{A1}
\end{aligned}$$

where $H_{\bar{a}} = H_{\bar{a}}(x)$.

Our results for the pseudoscalar singlet contribution reads

$$\begin{aligned}
c_{p,\text{sing}}^{(2)}|_{m_2} = n_m C_F T_F \left[\pi^2 \left(\frac{7t^3}{3(1+t^2)^3} + \frac{2tH_{\{4,1\}}}{1+t^2} \right) - \frac{4t^3 H_0}{(1+t^2)^2} + \frac{4t^3 H_0^2}{(1+t^2)^3} + \frac{16t^3 H_0 H_1}{(1+t^2)^3} \right. \\
+ \log(2) \left(-\frac{2t}{1+t^2} + \frac{16t^3 H_0}{(1+t^2)^3} + \frac{16t^3 H_1}{(1+t^2)^3} - \frac{16t^3 H_{-1}}{(1+t^2)^3} \right) + \left(\frac{4t}{1+t^2} - \frac{8tH_0^2}{1+t^2} \right) H_{\{4,1\}} \\
- \frac{16t^3 H_{0,1}}{(1+t^2)^3} + \left(-\frac{32t^3}{(1+t^2)^3} + \frac{24tH_0}{1+t^2} \right) H_{0,\{4,1\}} - \frac{32t^3 H_{1,\{4,1\}}}{(1+t^2)^3} - \frac{16t^3 H_{-1,0}}{(1+t^2)^3} \\
+ \frac{32t^3 H_{-1,\{4,1\}}}{(1+t^2)^3} - \frac{24tH_{0,0,\{4,1\}}}{1+t^2} + \frac{8t^3 \log^2(2)}{(1+t^2)^3} - \frac{3t\zeta(3)}{1+t^2} \\
\left. + i\pi \left\{ -\frac{(-1+t)t(1+t)}{(1+t^2)^2} - \frac{4t^3 H_0}{(1+t^2)^3} - \frac{8tH_0 H_{\{4,1\}}}{1+t^2} + \frac{12tH_{0,\{4,1\}}}{1+t^2} \right\} \right]. \tag{A2}
\end{aligned}$$

For the expansions around $x = 0$ and $x = 1$, we find

$$\begin{aligned}
c_{p,\text{sing}}^{(2)}|_{m_2, x \rightarrow 0} = n_m C_F T_F \left[x \left(-\log(2) - \frac{3\zeta(3)}{2} \right) + x^3 \left(-\frac{1}{8} + \frac{5\pi^2}{12} - \frac{\log(2)}{4} - \log^2(2) + \frac{1}{4}(1 + 8\log(2))\log(x) \right) \right. \\
\left. + i\pi \left\{ \frac{1}{2}x + x^3 \left(\frac{1}{8} + \log(2) - \log(x) \right) \right\} + \mathcal{O}(x^4) \right], \tag{A3}
\end{aligned}$$

$$\begin{aligned}
c_{p,\text{sing}}^{(2)}|_{m_2, x \rightarrow 1} = n_m C_F T_F \left[\frac{5\pi^2}{24} + \frac{1}{2}\pi^2 \log(2) - \frac{21\zeta(3)}{8} - \sqrt{y} \frac{\pi^2}{\sqrt{2}} + y \left(-1 - \frac{\pi^2}{8} + 2\log(2) - \frac{1}{2}\pi^2 \log(2) + \frac{21\zeta(3)}{8} \right) \right. \\
+ y^{3/2} \frac{7\pi^2}{12\sqrt{2}} + y^2 \left(\frac{1}{3} + \frac{3\pi^2}{8} - \frac{\log(2)}{3} \right) + y^{5/2} \frac{71\pi^2}{480\sqrt{2}} \\
+ i\pi \left\{ \frac{\pi^2}{8} + \sqrt{y}(\sqrt{2} - \sqrt{2}\log(2)) + y \left(-1 - \frac{\pi^2}{8} \right) + y^{3/2} \left(-\frac{11}{6\sqrt{2}} + \frac{7}{6\sqrt{2}}\log(2) \right) + \frac{y^2}{6} \right. \\
\left. + y^{5/2} \left(\frac{433}{240\sqrt{2}} + \frac{71}{240\sqrt{2}}\log(2) \right) \right\} + \mathcal{O}(y^3) \right], \tag{A4}
\end{aligned}$$

with $y = 1 - x$.

In the case of the singlet axial-vector current, we explicitly specify the flavor of the quark in the final state to bottom quark. Furthermore, we split the matching coefficient into the contributions from the strange and charm quarks $c_{a,\text{sing}}^{(2),s+c}|_{m_2}$ and the contribution from the bottom and top quarks $c_{a,\text{sing}}^{(2),b+t}|_{m_2}$.² For vanishing strange quark mass, we have

²Note that the contribution from up and down quarks vanishes since we assume that both quarks are massless.

$$\begin{aligned}
c_{a,\text{sing}}^{(2),s+c}|_{m_2} = n_m C_F T_F \left[\pi^2 \left(-\frac{t^2(1+25t^2+19t^4+9t^6)}{9(1+t^2)^4} + \frac{2t^2 H_1}{3(1+t^2)^2} + \frac{8t^2 H_{\{4,1\}}}{3(1+t^2)^2} + \frac{2t^2 H_{-1}}{(1+t^2)^2} \right) \right. \\
+ \log(2) \left(\frac{4t^2}{3(1+t^2)^2} - \frac{8t^4(5+2t^2+t^4)H_0}{3(1+t^2)^4} + \left(-\frac{4(1+2t^2+10t^4+2t^6+t^8)}{3(1+t^2)^4} + \frac{16t^2 H_{-1}}{3(1+t^2)^2} \right) H_1 \right. \\
+ \frac{8t^2 H_1^2}{3(1+t^2)^2} + \frac{4(1+2t^2+10t^4+2t^6+t^8)H_{-1}}{3(1+t^2)^4} + \left. \frac{8t^2 H_{-1}^2}{3(1+t^2)^2} \right) + \frac{4t^2(3+8t^2+3t^4)H_0}{3(1+t^2)^3} \\
+ \frac{4t^4(-1+2t^2+t^4)H_0^2}{3(1+t^2)^4} + \left(\frac{4(-3-6t^2-10t^4+2t^6+t^8)H_0}{3(1+t^2)^4} + \frac{8t^2 H_0^2}{3(1+t^2)^2} \right) H_1 \\
+ \frac{8t^2 H_0 H_1^2}{3(1+t^2)^2} + \left(-\frac{4(-3-6t^2-10t^4+2t^6+t^8)}{3(1+t^2)^4} - \frac{16t^2 H_0}{(1+t^2)^2} - \frac{16t^2 H_1}{3(1+t^2)^2} \right) H_{0,1} \\
+ \left(-\frac{4(3+8t^2+3t^4)}{3(1+t^2)^2} - \frac{32t^2 H_0^2}{3(1+t^2)^2} \right) H_{\{4,1\}} + \left(\frac{16t^4(5+2t^2+t^4)}{3(1+t^2)^4} + \frac{32t^2 H_0}{(1+t^2)^2} \right) H_{0,\{4,1\}} \\
+ \frac{8(1+2t^2+10t^4+2t^6+t^8)H_{1,\{4,1\}}}{3(1+t^2)^4} + \left(-\frac{8(1+2t^2+10t^4+2t^6+t^8)}{3(1+t^2)^4} - \frac{32t^2 H_1(t)}{3(1+t^2)^2} \right) H_{-1,\{4,1\}} \\
+ \left(-\frac{4(-3-6t^2-10t^4+2t^6+t^8)}{3(1+t^2)^4} + \frac{32t^2 H_0}{3(1+t^2)^2} + \frac{16t^2 H_1}{3(1+t^2)^2} \right) H_{-1,0} + \frac{80t^2 H_{0,0,1}}{3(1+t^2)^2} \\
- \frac{128t^2 H_{0,0,\{4,1\}}}{3(1+t^2)^2} + \frac{16t^2 H_{0,1,1}(t)}{3(1+t^2)^2} - \frac{32t^2 H_{1,1,\{4,1\}}}{3(1+t^2)^2} - \frac{80t^2 H_{-1,0,0}}{3(1+t^2)^2} - \frac{16t^2 H_{-1,0,1}}{3(1+t^2)^2} + \frac{32t^2 H_{-1,\{4,1\},1}}{3(1+t^2)^2} \\
+ \frac{16t^2 H_{-1,-1,0}}{3(1+t^2)^2} - \frac{32t^2 H_{-1,-1,\{4,1\}}}{3(1+t^2)^2} + \frac{4(-1+t)^2 t^2 (1+t) \log^2(2)}{3(1+t^2)^4} - \frac{5t^2 \zeta(3)}{(1+t^2)^2} \\
+ i\pi \left\{ \frac{\pi^2 t^2}{3(1+t^2)^2} + \frac{2t^2(2+t^2)(1+3t^2)}{3(1+t^2)^3} + \left(\frac{8t^4(2+2t^2+t^4)}{3(1+t^2)^4} + \frac{16t^2 H_{-1}}{3(1+t^2)^2} \right) H_0 \right. \\
+ \left(\frac{4(-1+t)(1+t)}{3(1+t^2)} + \frac{8t^2 H_0}{3(1+t^2)^2} \right) H_1 - \frac{32t^2 H_0 H_{\{4,1\}}}{3(1+t^2)^2} - \frac{4(-1+t)(1+t)H_{-1}}{3(1+t^2)} \\
\left. - \frac{8t^2 H_{0,1}}{(1+t^2)^2} + \frac{16t^2 H_{0,\{4,1\}}}{(1+t^2)^2} - \frac{8t^2 H_{-1,0}}{(1+t^2)^2} - \frac{4t^2 \log(2)}{3(1+t^2)} \right\} \Bigg], \tag{A5}
\end{aligned}$$

with $t = (1 - \sqrt{1 - x_c^2})/x_c$ and $x_c = m_c/m_b$. The expansion of $x_c \rightarrow 0$ is given by

$$c_{a,\text{sing}}^{(2),s+c}|_{m_2, x_c \rightarrow 0} = n_m C_F T_F \left[x_c^2 \left(-\frac{\pi^2}{36} + \frac{1}{3} \log^2(2) - \frac{5}{4} \zeta(3) + i\pi \left[\frac{\pi^2}{12} - \frac{1}{3} \log(2) \right] \right) + \frac{\pi^2}{3} x_c^3 + \mathcal{O}(x_c^4) \right]. \tag{A6}$$

Due to the large mass of the top quark, it is convenient to provide for $c_{a,\text{sing}}^{(2),b+t}|_{m_2}$ only the first few expansion terms in $x_t = m_b/m_t$. Our results read

$$\begin{aligned}
c_{a,\text{sing}}^{(2),b+t}|_{m_2} = n_m C_F T_F \left[\frac{55}{24} - \frac{3}{2} \log(x_t) + \pi^2 \left(\frac{19}{72} - \frac{2}{3} \log(2) \right) - x_t^2 \left(\frac{47}{216} + \frac{5}{18} \log(x_t) \right) \right. \\
\left. - x_t^4 \left(\frac{1337}{21600} + \frac{23}{108} \log(x_t) \right) + \mathcal{O}(x_t^6) \right]. \tag{A7}
\end{aligned}$$

In [10], computer-readable expressions for the four nonsinglet and the three singlet matching coefficients are provided. We include terms of order ϵ , which are needed for a future three-loop calculation.

- [1] A. Pineda, *Prog. Part. Nucl. Phys.* **67**, 735 (2012).
- [2] M. Beneke, Y. Kiyo, and K. Schuller, [arXiv:1312.4791](https://arxiv.org/abs/1312.4791).
- [3] M. Beneke, Y. Kiyo, and K. Schuller, *Phys. Lett. B* **658**, 222 (2008).
- [4] A. Czarnecki and K. Melnikov, *Phys. Rev. Lett.* **80**, 2531 (1998).
- [5] M. Beneke, A. Signer, and V. A. Smirnov, *Phys. Rev. Lett.* **80**, 2535 (1998).
- [6] P. Marquard, J. H. Piclum, D. Seidel, and M. Steinhauser, *Phys. Rev. D* **89**, 034027 (2014).
- [7] M. Beneke, Y. Kiyo, and A. A. Penin, *Phys. Lett. B* **653**, 53 (2007).
- [8] M. Beneke, Y. Kiyo, P. Marquard, A. Penin, J. Piclum, D. Seidel, and M. Steinhauser, *Phys. Rev. Lett.* **112**, 151801 (2014).
- [9] M. Beneke, A. Maier, J. Piclum, and T. Rauh, *Nucl. Phys.* **B891**, 42 (2015).
- [10] <https://www.ttp.kit.edu/preprints/2021/ttp21-012/>.
- [11] M. Beneke and V. A. Smirnov, *Nucl. Phys.* **B522**, 321 (1998).
- [12] V. A. Smirnov, *Springer Tracts Mod. Phys.* **177**, 1 (2002).
- [13] A. V. Smirnov and F. S. Chuharev, *Comput. Phys. Commun.* **247**, 106877 (2020).
- [14] R. N. Lee, [arXiv:1212.2685](https://arxiv.org/abs/1212.2685).
- [15] C. Meyer, *Comput. Phys. Commun.* **222**, 295 (2018).
- [16] E. Remiddi and J. A. M. Vermaseren, *Int. J. Mod. Phys. A* **15**, 725 (2000).
- [17] A. G. Grozin, P. Marquard, A. V. Smirnov, V. A. Smirnov, and M. Steinhauser, *Phys. Rev. D* **102**, 054008 (2020).
- [18] D. J. Broadhurst, N. Gray, and K. Schilcher, *Z. Phys. C* **52**, 111 (1991).
- [19] S. Bekavac, A. Grozin, D. Seidel, and M. Steinhauser, *J. High Energy Phys.* **10** (2007) 006.
- [20] A. I. Davydychev and A. G. Grozin, *Phys. Rev. D* **59**, 054023 (1999).
- [21] M. Fael, K. Schönwald, and M. Steinhauser, *J. High Energy Phys.* **10** (2020) 087.
- [22] B. A. Kniehl, A. Onishchenko, J. H. Piclum, and M. Steinhauser, *Phys. Lett. B* **638**, 209 (2006).
- [23] S. A. Larin, *Phys. Lett. B* **303**, 113 (1993).
- [24] J. Vermaseren, *Int. J. Mod. Phys. A* **14**, 2037 (1999); E. Remiddi and J. Vermaseren, *Int. J. Mod. Phys. A* **15**, 725 (2000); J. Blümlein, *Comput. Phys. Commun.* **180**, 2218 (2009); J. Ablinger, Diploma Thesis, J. Kepler University Linz, 2009; J. Ablinger, J. Blümlein, and C. Schneider, *J. Math. Phys. (N.Y.)* **52**, 102301 (2011); **54**, 082301 (2013); J. Ablinger, Ph.D. Thesis, J. Kepler University Linz, 2012; J. Ablinger, J. Blümlein, and C. Schneider, *J. Phys. Conf. Ser.* **523**, 012060 (2014); J. Ablinger, J. Blümlein, C. Raab, and C. Schneider, *J. Math. Phys. (N.Y.)* **55**, 112301 (2014); J. Ablinger, *Proc. Sci.*, LL2014 (2014) 019 [[arXiv:1407.6180](https://arxiv.org/abs/1407.6180)]; [arXiv:1606.02845](https://arxiv.org/abs/1606.02845); *Proc. Sci.*, RADCOR2017 (2017) 069 [[arXiv:1801.01039](https://arxiv.org/abs/1801.01039)]; LL2018 (2018) 063; [arXiv:1902.11001](https://arxiv.org/abs/1902.11001).
- [25] J. H. Piclum, Heavy quark threshold dynamics in higher order, Dissertation, Hamburg University, 2007.
- [26] J. Ablinger, J. Blümlein, P. Marquard, N. Rana, and C. Schneider, *Nucl. Phys.* **B939**, 253 (2019).
- [27] C. Schneider, Sémin. Lothar. Combin. **B56b**, 1 (2007); C. Schneider, in: *Computer Algebra in Quantum Field Theory: Integration, Summation and Special Functions*, Texts and Monographs in Symbolic Computation, edited by C. Schneider and J. Blümlein (Springer, Wien, 2013), p. 325.
- [28] S. Gerhold, Uncoupling systems of linear ore operator equations, Diploma Thesis, RISC, J. Kepler University, Linz, 2002.
- [29] D. Eiras and J. Soto, *Phys. Lett. B* **491**, 101 (2000).
- [30] A. H. Hoang, [arXiv:hep-ph/0008102](https://arxiv.org/abs/hep-ph/0008102).
- [31] M. Beneke, Y. Kiyo, A. Maier, and J. Piclum, *Comput. Phys. Commun.* **209**, 96 (2016).
- [32] C. Ayala, G. Cvetič, and A. Pineda, *J. High Energy Phys.* **09** (2014) 045.
- [33] A. Pineda, *Phys. Rev. D* **66**, 054022 (2002).
- [34] A. Pineda, *Phys. Rev. D* **65**, 074007 (2002).
- [35] F. Jegerlehner, *Nuovo Cimento C* **034S1**, 31 (2011).
- [36] P. A. Zyla *et al.* (Particle Data Group Collaboration), *Prog. Theor. Exp. Phys.* **2020**, 083C01 (2020).
- [37] F. Herren and M. Steinhauser, *Comput. Phys. Commun.* **224**, 333 (2018).
- [38] K. G. Chetyrkin, J. H. Kuhn, A. Maier, P. Maierhofer, P. Marquard, M. Steinhauser, and C. Sturm, *Phys. Rev. D* **80**, 074010 (2009).
- [39] D. Hatton, C. T. H. Davies, J. Koponen, G. P. Lepage, and A. T. Lytle, *Phys. Rev. D* **103**, 054512 (2021).
- [40] M. Beneke, *Phys. Lett. B* **434**, 115 (1998).
- [41] M. Beneke, Y. Kiyo, and K. Schuller, *Nucl. Phys.* **B714**, 67 (2005).
- [42] B. A. Kniehl, A. A. Penin, A. Pineda, V. A. Smirnov, and M. Steinhauser, *Phys. Rev. Lett.* **92**, 242001 (2004); **104**, 199901(E) (2010).
- [43] D. Hatton, C. T. H. Davies, B. Galloway, J. Koponen, G. P. Lepage, and A. T. Lytle (HPQCD Collaboration), *Phys. Rev. D* **102**, 054511 (2020).